Research Article | Vol. 26, No. 21 | 15 Oct 2018 | OPTICS EXPRESS 27545
Optics EXPRESS

High-performance composite Ag-Ni mesh based flexible transparent conductive film as multifunctional devices

SU SHEN,[1,2] SHI-YU CHEN,[1,2] DONG-YU ZHANG,[3] AND YAN-HUA LIU[1,2,*]

[1]School of Optoelectronic Science and Engineering & Collaborative Innovation Center of Suzhou Nano Science and Technology, Soochow University, Suzhou 215006, China
[2]Key Lab of Advanced Optical Manufacturing Technologies of Jiangsu Province & Key Lab of Modern Optical Technologies of Education Ministry of China, Soochow University, Suzhou 215006, China
[3]Suzhou Institute of Nano-Tech and Nano-Bionics, Chinese Academy of Sciences Suzhou 215123, China
*yhliu@suda.edu.cn

Abstract: Conventional fabrication methods for realization of metal mesh (MM) based transparent conductive film (TCF) are not economic and environmentally friendly. By combination of the scrape and selective electroplating techniques, a vacuum sputtering/evaporation-free process is explored for fabrication of high-performance MM based TCF. The fabricated TCF exhibits ultra-low sheet electrical resistance (Rs = 0.07 Ω sq−1) at average transmittance of 83% in visible region. The sample cannot only exhibit high heating temperatures (140 °C) at low input voltage (1.5 V) with fast and stable thermal response but provide high electromagnetic interference shielding efficiency (EMI SE) more than 43 dB in X-band. The processing chain provides a robust, powerful and scalable platform, which may open up a new avenue for realizing multifunctional TCF in diverse applications.

1. Introduction

Over the last ten years, rapid advances in the design of flexible electric/optoelectronic devices, make TCF an essential component for a variety of applications in information (display, touch screen, electromagnetic interference shielding) and energy (thin film solar cell, organic light-emitting diode, architectural and window glass) technologies. Conventional indium tin oxide (ITO) material is considered prohibitive, particularly in large area and flexible applications for some innate drawbacks of the ITO electrode such as brittleness due to its ceramic nature and increasing price due to the scarcity of indium [1,2]. Alternatives to ITO that are widely studied include carbon-based materials [3–7], organic-inorganic hybrid materials [8–11] and metals [12–20]. Carbon-based materials (carbon nanotube and graphene etc.) can improve TCF flexibility, but are still limited to small-scale due to high cost and energy-consumption. Organic or inorganic semiconductors, such as Al and Ga doped in zinc or tin oxide, have been tried out as transparent heater requiring high driven voltage or suffering from relatively high resistivity due to the high work function. In contrast, metal is preferred option material when considering high conductivity, stability, and low-cost. For patterning metallic network as transparent conductors, a variety of fabrication techniques have been investigated. Silver nanowires (NWs) demonstrate several drawbacks such as facile nanowire breakdown on application of a high DC voltage, easy oxidation when exposed to harsh environments, resulting in increased surface resistivity, and high resistance among wire junctions causing non-homogeneous temperature profiles. Metal-mesh electrodes with regular or randomly patterned micro-grooves seem more promising since there is no such problem of high wire-to-wire junction resistance. Furthermore, the transmittance and electrical conductivity can be tuned in a wide range by changing the line width, line spacing and metal thickness.

#342462 https://doi.org/10.1364/OE.26.027545
Journal © 2018 Received 15 Aug 2018; revised 27 Sep 2018; accepted 27 Sep 2018; published 5 Oct 2018

Optics EXPRESS

The state-of-the-art micro- and nanofabrication techniques, such as photolithography [21–23], cracking template [24,25], jet printing [26] and nanosphere lithography method [27], have been employed for formation of grid metallic patterns. However, the above-mentioned methods involve time-consuming vacuum-based process for depositing metal from the vapor phase or lift-off technique for removing extra materials, which are not economic and environmentally friendly. It remains a challenge to simultaneously overcome multiple issues such as further simplification of the manufacturing process by eliminating photolithography of etching steps, reduction of facility cost, increase of throughput, and improvement of electrical and optical performance.

Herein, we report realization of flexible composite MM based TCF through an additive manufacturing approach with parallel processing capability, as well as remarkable simplicity and fully controllable flexibility to tailor the transmittance and sheet resistance. The embedded Ag grid is formed by the scrape technique and Ni is selectively deposited in the conductive network via the action of an electric current to further enhance conductivity without complicate and cost processes such as etching and lift-off process. Furthermore, geometric factors such as line width, height, and morphology can be independently controlled, and as a result, the electrical properties can be widely tuned. The Ag paste attaches to the groove bottom, providing conductive mesh for the selective deposition of nickel. That's to say, the nickel is well constrained by the groove during the electroforming process. The sheet resistance reduces from 0.8 Ω sq^{-1} to 0.07 Ω sq^{-1} while the optical transmittance remains unchanged (~83%). The composite Ag-Ni conductive mesh is embedded in UV resin, which shows appropriate mechanical robustness. There is no significant degradation in electrical conductivity (<10% after bending test) due to the embedded structure. As transparent heater, the TCF exhibits high heating temperatures (140 °C) with low input voltage (1.5 V), short response time (T<50 s), and low power consumption (160.6 °C cm^2 W^{-1}), as well as stability after repeated use. As transparent EMI shielding material, the TCF exhibits high SE (>43 dB) in X-band, while the rising temperature (from 25 °C to 80 °C) has negligible influence on shielding effect. By combination of the soft nanoimprinting, the scrape technique and the selectively electrochemical deposition, the simplification of the manufacturing process and improvement of the overall electrical and optical performance make the composite MM based TCF suitable as high-performance multifunctional optoelectronic film device in terms of scalability and cost.

2. Fabrication of the composite Ag-Ni mesh film

Figure 1(a) shows the fabrication process of the composite Ag-Ni mesh based TCF. Firstly, a layer of photoresist (RZJ-390PG, Ruihong Electronic Chemical Co., LTD) is spin-coated on glass substrate. An in-house built digital micro-mirror device (DMD) based maskless lithography system is used for direct-writing the micro-grooves on photoresist [28]. There are several advantages for the system, such as allowing arbitrary pattern, high-resolution, parallel processing inherently, non-contact working mode, easy-to-obtain high aspect-ratio microstructure and much higher efficiency than that of e-beam lithography.

Secondly, the micro-groove structure is replicated to a soft mold through nanoimprinting technique. The photoresist layer is illuminated under a UV light for aging-treatment, and then the modified polyurethane acrylate (PUA) (D10, Shanghai PhiChem Material Co., Ltd) is drop-dispensed on a flexible poly (ethylene terephthalate) (PET) (4300, Toyobo Japan) film with a thickness of 100 μm for imprinting. Then, the PET film with the cured PUA is mechanically peeled off from the photoresist mold. It is used as a soft patterned stamp composed of protrusion mesh on the surface. Sufficient mechanical strength of the cured PUA guarantees the replication fidelity and its relatively low surface energy reduces the demolding force. The soft PUA mold can be used for several hundred times. Then, it is extruded on the dispersed UV-curable resin (D25, Shanghai PhiChem Material Co., Ltd) on a substrate for exposure. The imprinting pressure is typically less than 0.3 MPa due to the low viscosity of

Optics EXPRESS

liquid UV resin. For the PUA mold, it takes about 20 s to cure the resist under a 365 nm light-emitting diode with an intensity of 1000 mW/cm^2 at a distance of 1 cm. For the UV mesh network, it takes about 20 s to cure the resist under the above same condition.

Thirdly, the Ag paste ink (concentration of 70%, viscosity of 25 cps, and particle diameter in the range of 200 to 300 nm, Suzhou Betely Polymer Materials Co., Ltd) is filled into the micro-grooves through the scrape technique. After 20 min sintering at 80 °C, the embedded conductive Ag mesh is formed in the UV resin. A wiping process with nontoxic organic solvents can be employed to clean the surface.

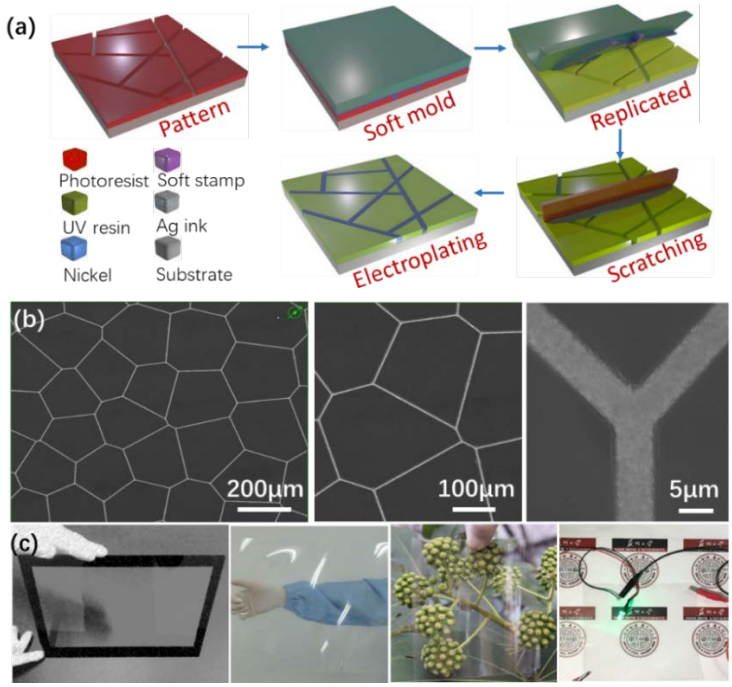

Fig. 1. Schematic illustration of the fabrication process of the composite Ag-Ni mesh based TCF. (a) Spin-coating photoresist and laser direct writing of micro-grooves pattern. Pattern replication from the photoresist to a soft mold, then the microstructure is subsequently replicated with the soft stamp via UV nanoimprinting. Dispersing and scratching Ag ink into the microgrooves. Selectively electroplating Ni on the top of Ag mesh to form conductive grid. (b) SEM image of the patterned grid. The enlarged images indicate the detail of the composite Ag-Ni mesh (left to right). (c) Photograph of the large-area composite Ag-Ni mesh based TCFs (size: 40 cm x 30 cm), indicating its superior optical transparency and electric conductivity (left to right).

Finally, nickel is selectively deposited on the top surface of the Ag mesh by electroplating. 150 mL Ni plating solution composed of 4 g $Ni(SO_3NH_2)_2$ $4H_2O$, 0.6 g $NiCl_2$ $6H_2O$, and 0.3 g HBO_3 in distilled water, is used for the electroplating deposition. A plating set-up (China Electronics Technology Group Corporation, DDT-3) is used in the process. In the electroforming process, the Ag mesh serves as cathode and Ni is grown on it. By applying potential between the two electrodes, Ni was deposited over the Ag mesh to form the composite MM grid. Cathode current density is 0.5 A/m^2. The thickness of the deposited Ni can be controlled by the duration time. Then, the obtained composite MM based TCF was thoroughly washed with deionized water to remove the residual electrolyte and dried in ambient air. The use of a solvent-containing development agent ensures the surface completely free of grease and ready for plating. Figure 1(b) shows the morphological pattern of the conductive composite Ag-Ni mesh. The fabricated large-area film exhibits superior optical transparency and electric conductivity, as shown in Fig. 1(c). Compared with the

Optics EXPRESS

methods mentioned in [21,22], due to the combination of the nanoimprinting lithography, the scraping technique, and the electroplating, the proposed process is easier to be scaled up to mass-production of high performance TCF.

3. Results and discussions

3.1 Electrical, optical and mechanical characterization of the composite Ag-Ni mesh based TCF

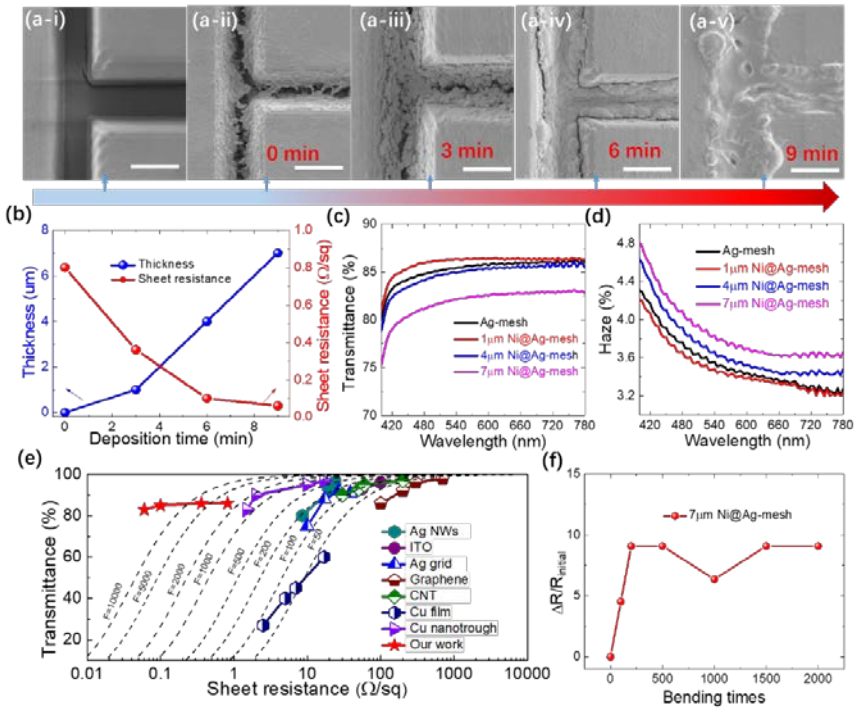

Fig. 2. (a-i) Surface profiles of the micro-grooves and (a-ii~v) of the conductive mesh grid after Ni deposition treatment of 0, 3 min, 6 min, and 9 min. The scale bar is 5 μm. (b) Deposition thickness and sheet resistance of the Ni as a function of the deposition time. (c) Transmittance and (d) haze spectrum of the composite Ag-Ni mesh with a period of 160 μm. (e) Optical transmittance versus the corresponding sheet resistance for the TCF. Performances of commercial ITO films, CNTs [5], graphene [6], Ag NWs [29], Ag grids [30], Cu film [31], and Cu nanotrough [32] are also shown for comparison. (f) The normalized variation in sheet resistance versus the number of cycles of the repeated bending to radii of 2.5 mm.

The imprinted micro-groove is 4 μm wide and 8 μm deep, whose scanning electronic beam (SEM) (FESEM: JEOL, JSM-5400, USA) pictures are shown in Figs. 2(a-i)-2(a-v). Embedded conductive mesh is formed by filling the Ag ink into the trench through the scrape technique, as shown in Figs. 2(a-i)-2(a-ii). Ag nanoparticles attach to the bottom of the grooves. It exhibits relatively high sheet resistance (0.8 Ω sq^{-1}) owing to the contact resistance between the Ag nanoparticles and the average transmittance is about 85% at this stage. The sheet resistance of the fabricated samples R_s was measured using a four-point probe (CMT SR2000, A. I. T.). The conductivity can be greatly reduced by selectively depositing Ni metal into the imprinting defined Ag trenches using electroforming process, since the voids between the Ag particles can be bridged by the deposited Ni.

The Ni is constrained in the groove by carefully optimizing the deposition time. The surface profiles of the composite Ag-Ni mesh with 3 min, 6 min and 9 min deposition time at a step of 3 min are shown in Figs. 2(a-iii)-2(a-v). As depicted in Fig. 2(b), the thickness of the nickel increases from 0 to 7 μm, and meanwhile the R_s of the composite Ag-Ni mesh TCEs

Optics EXPRESS

decrease drastically from 0.8 Ω sq^{-1} to 0.07 Ω sq^{-1}. If the deposition time is longer than 10 min, the nickel overflows from the groove, resulting in lower transparency. It can be attributed to the well-filled Ag mesh, which facilitates more efficient ion transport and transfer over the entire Ni network surface and thus boosts the electrochemical performance.

As shown in Fig. 2(c), as the deposited Ni is confined in the grooves, the measured sheet resistance decreases an order of magnitude to less than 0.07 Ω sq^{-1}, but there is no obvious decrease in transmittance. When the deposited Ni broadens out of the patterned groove, as shown in Fig. 2(a-v), the transmittance decreases from 85% to 83% over the 400 nm - 800 nm spectra regime (Lambda 750 UV–VIS spectrometer, Perkin Elmer, USA). There is no dispersion in transmission spectrum with the introduction of the MM. It can be concluded that if the Ni is locally deposited in the micro-groove, its influence on the optical characteristics is negligible. The widening conductive mesh leads to an increase in the average optical haze factor from 3.5% to 4.0%, as shown in Fig. 2(d). The Ni thickness on the Ag mesh can be easily controlled by tuning the electro-deposition time without any vacuum or specialized equipment due to its additive manufacturing nature, provide a feasible way to greatly improve the electric conductivity.

Figure 2(e) shows compilation of optoelectronic properties of various TCFs, including our composite Ag-Ni mesh, compared to other TCF such as the commercial ITO films, CNTs [5], graphene [6], Ag NWs [29], Ag grids [30], Cu film [11], and Cu nanotrough [13]. The lines represent parameters corresponding to a fixed figure of merit F, which is detailed described in [13]. Our composite Ag-Ni mesh based TCF have transmittance ranging from 83% (Rs = 0.07 Ω sq^{-1}) to 85% (Rs = 0.8 Ω sq^{-1}). The red line denotes the F values for our samples, which represents colossal F = 1 000 and 10 000. The composite Ag-Ni mesh based TCF shows better optoelectronic properties than other schemes. Increasing the thickness of the deposited nickel layer can significantly improve the conductivity, leading to a superior overall optoelectronic performance.

To quantitatively evaluate the impact of bending on the electrical performance, the TCF with 7 μm thickness nickel is measured after successive 2000 bending cycles. Figure 2(f) shows the variation of the sheet resistance $\Delta R / R_{initial}$ as a function of bending cycles with 2.5 mm bending radii. ΔR and $R_{initial}$ is the measured variation and initial resistance, respectively. By examining the TCF after bending regime, we found there is no physical damage on the surface and the electrical conductivity deteriorates less than 10%. The appropriately mechanical stability is attributing to the embedded configuration of the proposed composite Ag-Ni mesh based TCF. The strong adhesion between the Ag and Ni helps to preserve electrical contacts under extreme bending stress, which is essential for flexible optoelectronic application.

3.2 Composite Ag-Ni mesh based TCF as transparent heater

High-performance transparent heater requires a fast thermal response, high transmittance in the visible range, uniformly heated surface, large-area coverage and flexible ultra-thin substrate [31–34]. A transparent heater based on the composite Ag-Ni mesh is constructed on a 100 μm-thick PET substrate. Figure 3(a) shows the thermal response of the samples with different plating nickel thickness (0, 1, 4, 7 μm) under external applied voltage 1.5 V. The temperature of the transparent film was measured using a FLIR ONE infrared thermal imager (FLIR Systems, USA). The temperature of the composite Ag-Ni mesh based TCF increased rapidly as soon as the input voltage is applied. Lower sheet resistance leads to better heating efficiency, which means a faster heating rate and higher thermal equilibrium temperature. The maximum temperature was 110 °C under 1.5 V input voltage. Figure 3(b) shows the temperature-time profiles of the heater under different input voltage (0.5, 0.8, 1.0, 1.2 and 1.5 V). After about 50 s, the maximum temperature 150 °C is reached.

Optics EXPRESS

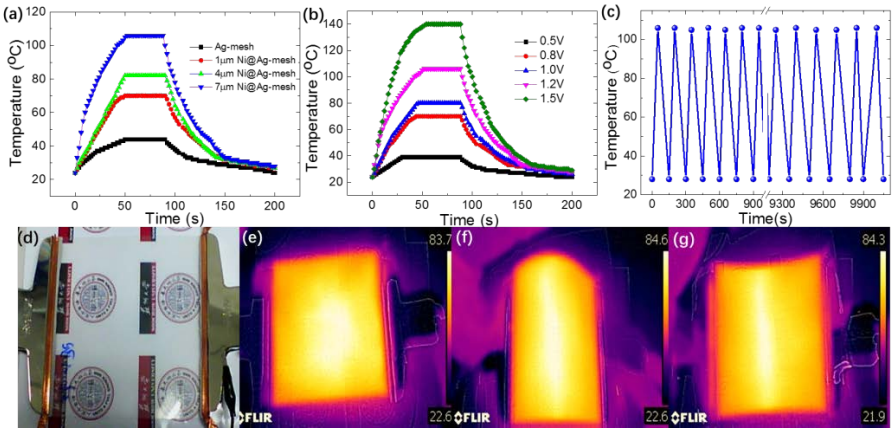

Fig. 3. (a) Temperature-time profiles of the composite Ag-Ni mesh based TCF heaters under different input voltages. (b) Temperature profiles of the proposed TCF at applied voltages of 0.5, 0.8, 1.0, 1.2 and 1.5 V. (c) Switching cycles under an applied voltage of 2 V. (d) Picture of the experimental setup. (e-g) Thermal images in bent positions while an input bias was applied.

The remarkable performance is attributed to the ultralow sheet resistance because of the absence of cross-bar junctions in the composite Ag-Ni mesh networks. In order to demonstrate the electrical stability of the composite Ag-Ni mesh based TCF, the stability test was conducted at the operating voltage of 2 V. The duration and spacing time were 50 s respectively. The temperature was monitored at 150 s intervals. After repeated over 60 cycles, the investigated TCF still performs well as depicted in Fig. 3(c). The electroplating nickel on the top can prevents Ag from oxidation in a hostile environment. The experimental setup is shown in Fig. 3(d) using a DC power supply through an Ag side contact. The temperature distribution images were captured by using an infrared camera in bent positions, as shown in Figs. 3(e)-3(g). To our knowledge, it is the minimum input voltage for achieving such high temperature ever reported. It is clear that the investigated composite Ag-Ni mesh based TCF shows uniform heat distribution over the whole area while maintaining flexibility and transparency, which can possibly expand a variety of applications, for instance the defrosting and deicing window used typically in LCD panels, vehicles, advertisement boards as well as in display screens of teller machines, avionics etc.

3.3 Composite Ag-Ni mesh based TCF as transparent EMI film

Owing to the superior optical transparency and electrical behavior, the composite Ag-Ni mesh based TCF is considered the best candidate as not only transparent heater, but also EMI shielding material, which is becoming more and more important for acting as a shield against the penetration of the radiation energy through the shield in the optoelectronic applications. The fabricated TCF with an average line-spacing of 160 μm is used for test. Figure 4(a) shows the schematic of the EMI SE measurement setup, which is composed of a vector network analyzer, transmitter antenna and receiver antenna. An external DC source is contacted to the sample for the purpose of heating. The EMI SE is expressed by the ratio in decibels (dB) between incident power (Pi) and transmitted power (Pt): SE(dB) = −10log (Pt/Pi) [31]. Experimental results are shown in Fig. 4(b). Plastic substrates are non-conducting and transparent to electromagnetic wave in gigahertz region. All the samples provided efficient shielding effect in X-band. For the composite Ag-Ni mesh based TCF, the maximum SE can reach ~43 dB. However, for the only Ag mesh based TCF, the measured EMI SE peak value is drastically decreased to ~28 dB. The measured results are very similar to the simulation results illustrated in Fig. 4(c). The theoretical SE of the Ag mesh is greater than the measured results for the relatively larger contact resistance between Ag nanoparticles

Optics EXPRESS

than pure Ag. By increasing the thickness of the electroplating Ni, the composite mesh grid is well defined and the EMI SE improves as well.

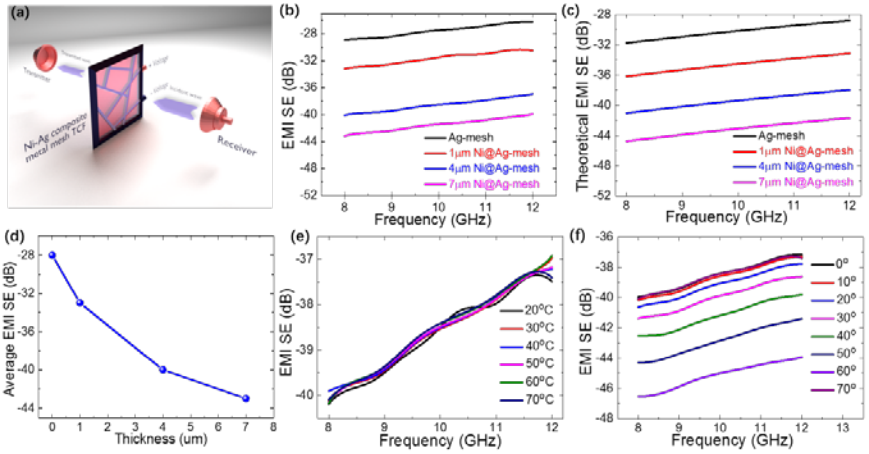

Fig. 4. Shielding performances of the composite Ag-Ni mesh based TCF. (a) Schematic illustration of the EMI SE measurement setup. (b) EMI SE curves of the composite Ag-Ni mesh based TCFs with different deposition thickness. (c) Simulation results of the SE. (d) Average EMI SE of the samples. (e) Measured EMI SE at elevated temperature from 20 °C to 70 °C. (f) EMI SE curves as a function of incident angle.

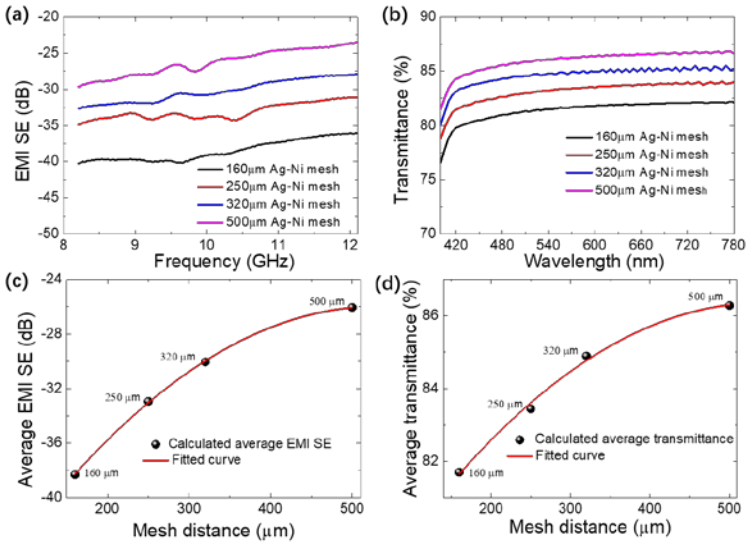

Fig. 5. (a) EMI SE curves and (b) transmittance of the TCF with an average mesh distance 160, 250, 320, and 500 μm, respectively. Fitting curve of the average (c) EMI SE and (d) transmittance of the TCF with different Ag-Ni mesh distance.

The average EMI SE of the sample with Ni is certainly superior to that with only Ag layer, as shown in Fig. 4(d). Figure 4(e) shows that the fabricated TCF has brilliant EMI shielding effect in the elevated temperature region. It can be seen that the variation of the temperature from 20 °C to 70 °C has negligible influence on the EMI SE. The multifunctional film based such composite Ag-Ni mesh based TCF still keeps the EMI SE performance while heating, which is vital to military applications for its defrosting or defogging capability.

Optics EXPRESS

Meanwhile, when increasing the incident angle, the SE value is increased as well, as shown in Fig. 4(f).

Furthermore, we investigate the influence of the mesh arrangement on the EMI SE and transmittance of the TCF. Figures 5(a)-5(b) show the EMI SE and transmittance of the composite TCF with an average mesh distance of 160, 250, 320, and 500 μm, respectively. The dimension sizes of the micro-grooves in the samples are the same as 4 μm wide and 8 μm deep. A 4 μm-thick layer of Ni is selectively deposited on the top of the Ag mesh. It can be clearly seen that as the average mesh distance increases, the EMI SE decreases and transmittance becomes higher. The average EMI SE (frequency ranging from 8 GHz to 12 GHz) and average transmittance (wavelength ranging from 400 nm to 700 nm) of the TCF with average mesh distance of 160, 250, 320, and 500 μm are depicted in Figs. 5(c) and 5(d), according to the measured results in Figs. 5(a) and 5(b). It can be deduced from the fitting curves that the average transmittance is proportional to the average mesh distance, whereas the EMI SE is the opposite. The sheet resistance is measured as 0.1, 0.25, 0.42 and 1.02 Ω sq^{-1}, which is also in inversely proportional to the filling factor of mesh grid. For practical applications, it needs to make a compromise between optical transparency, electrical conductivity, and EMI SE.

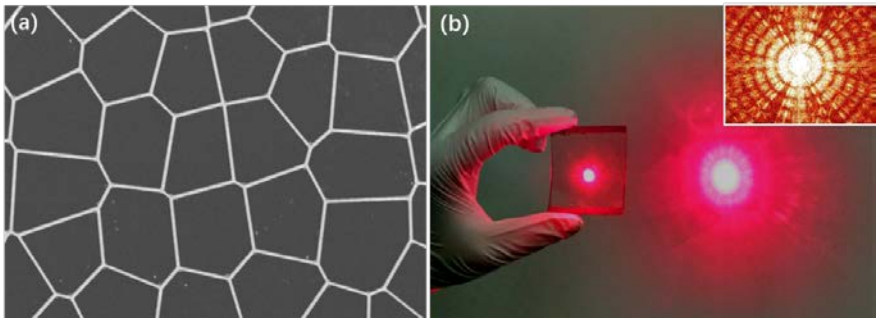

Fig. 6. (a) Picture of the grid pattern. (b) Optical diffraction pattern of a laser beam through the MM based TCF. The inset is the theoretical prediction by FFT.

Additionally, the adoption of the randomized MM has a certain impact on optical performance in the visible region. The randomly distributed mesh grid with an average line-spacing of 160 μm is shown in Fig. 6(a). It exhibits highly centered diffraction patterns around the central point and faint high-order light spots (i.e., stray light) when being irradiated with a laser pointer, as shown in Fig. 6(b). The inset shows the numerical simulation result calculated by the fast Fourier transform algorithm, which is well consistent with the experimental result. The random-pattern metal-mesh can perfectly eliminate moire fringes and “ghosts” that seriously influence the visual effect and optical imaging in regularly periodic metal grids.

4. Summary

In summary, we propose and experimentally demonstrate additive manufacturing of high-performance composite Ag-Ni mesh based TCF. Combined the scrape technique with the selected electroplating technique, Ni is selectively deposited on the embedded Ag mesh to enhance the electrical conductivity without expensive vacuum process. The fabricated TCF has a high figure of merit F of 10^4 and is put forward as flexible multifunctional material as both transparent heater and EMI shielding film. Low input voltage of 1.5 V is realized for achieving a high temperature of 150 °C. The TCF exhibits high shielding efficiency (>43 dB) in X-band, while the rising temperature has negligible influence on shielding effect. The selectively deposited Ni provides the materials with stable or even enhanced permittivity, which is attractive for realization of superior optoelectronic characteristics. The additive

Optics EXPRESS

nature of the proposed method has demonstrated great potential in terms of scalability and cost for fabrication of the multifunctional TCF with the advantages of high conductivity, light-weight, and good corrosion resistance.

Funding

National Key Research and Development Program of China (Project No. 2017YFB0404501); the National Natural Science Foundation of China (Nos 61575133, 61405133); the Natural Science Foundation of Jiangsu Province (No. BK20181166). Natural Science Foundation of the Jiangsu Higher Education Institutions of China (No. 18KJB510040); National High Technology Research and Development Program 863 (No. 2015AA042401); Project funded by the Priority Academic Program Development of Jiangsu Higher Education Institutions (PAPD).

References

1. K. Ellmer, "Past achievements and future challenges in the development of optically transparent electrodes," Nat. Photonics **6**(12), 808–816 (2012).
2. T. M. Barnes, M. O. Reese, J. D. Bergeson, B. A. Larsen, J. L. Blackburn, M. C. Beard, J. Bult, and J. van de Lagemaat, "Comparing the fundamental physics and device performance of transparent, conductive nanostructured networks with conventional transparent conducting oxides," Adv. Energy Mater. **2**(3), 353–360 (2012).
3. H. Z. Geng, K. K. Kim, K. P. So, Y. S. Lee, Y. Chang, and Y. H. Lee, "Effect of acid treatment on carbon nanotube-based flexible transparent conducting films," J. Am. Chem. Soc. **129**(25), 7758–7759 (2007).
4. S. Bae, H. Kim, Y. Lee, X. Xu, J.-S. Park, Y. Zheng, J. Balakrishnan, T. Lei, H. R. Kim, Y. I. Song, Y. J. Kim, K. S. Kim, B. Ozyilmaz, J.-H. Ahn, B. H. Hong, and S. Iijima, "Roll-to-roll production of 30-inch graphene films for transparent electrodes," Nat. Nanotechnol. **5**(8), 574–578 (2010).
5. A. Kaskela, A. G. Nasibulin, M. Y. Timmermans, B. Aitchison, A. Papadimitratos, Y. Tian, Z. Zhu, H. Jiang, D. P. Brown, A. Zakhidov, and E. I. Kauppinen, "Aerosol-synthesized SWCNT networks with tunable conductivity and transparency by a dry transfer technique," Nano Lett. **10**(11), 4349–4355 (2010).
6. R. Menzel, S. Barg, M. Miranda, D. B. Anthony, S. M. Bawaked, M. Mokhtar, S. A. Al-Thabaiti, S. N. Basahel, E. Saiz, and M. S. P. Shaffer, "Joule heating characteristics of emulsion-templated graphene aerogels," Adv. Funct. Mater. **25**(1), 28–35 (2015).
7. D. S. Hecht, L. Hu, and G. Irvin, "Emerging transparent electrodes based on thin films of carbon nanotubes, graphene, and metallic nanostructures," Adv. Mater. **23**(13), 1482–1513 (2011).
8. D. Angmo and F. C. Krebs, "Flexible ITO-Free polymer solar cells," J. Appl. Polym. Sci. **129**(1), 1–14 (2013).
9. J. H. Kim, B. Du Ahn, C. H. Kim, K. A. Jeon, H. S. Kang, and S. Y. Lee, "Heat generation properties of Ga doped ZnO thin films prepared by rf-magnetron sputtering for transparent heaters," Thin Solid Films **516**(7), 1330–1333 (2008).
10. H. Kang, S. Jung, S. Jeong, G. Kim, and K. Lee, "Polymer-metal hybrid transparent electrodes for flexible electronics," Nat. Commun. **6**(1), 6503 (2015).
11. R. J. Pelaez, T. Kuhn, C. E. Rodriguez, and C. N. Afonso, "Dynamics of laser induced metal nanoparticle and pattern formation," Appl. Phys. Lett. **106**(6), 061914 (2015).
12. Y. Li, K. Tsuchiya, H. Tohmyoh, and M. Saka, "Numerical analysis of the electrical failure of a metallic nanowire mesh due to Joule heating," Nanoscale Res. Lett. **8**(1), 370 (2013).
13. H. Wu, D. Kong, Z. Ruan, P.-C. Hsu, S. Wang, Z. Yu, T. J. Carney, L. Hu, S. Fan, and Y. Cui, "A transparent electrode based on a metal nanotrough network," Nat. Nanotechnol. **8**(6), 421–425 (2013).
14. H. J. Kim, Y. Kim, J. H. Jeong, J. H. Choi, J. Lee, and D. G. Choi, "A cupronickel-based micromesh film for use as a high-performance and low-voltage transparent heater," J. Mater. Chem. A Mater. Energy Sustain. **3**(32), 16621–16626 (2015).
15. O. S. Hutter and R. A. Hatton, "A hybrid Copper:Tungsten suboxide window electrode for organic photovoltaics," Adv. Mater. **27**(2), 326–331 (2015).
16. E. C. Garnett, W. Cai, J. J. Cha, F. Mahmood, S. T. Connor, M. Greyson Christoforo, Y. Cui, M. D. McGehee, and M. L. Brongersma, "Self-limited plasmonic welding of silver nanowire junctions," Nat. Mater. **11**(3), 241–249 (2012).
17. D. Langley, G. Giusti, C. Mayousse, C. Celle, D. Bellet, and J.-P. Simonato, "Flexible transparent conductive materials based on silver nanowire networks: a review," Nanotechnology **24**(45), 452001 (2013).
18. J. Jang, H.-G. Im, J. Jin, J. Lee, J.-Y. Lee, and B.-S. Bae, "A flexible and robust transparent conducting electrode platform using an electroplated silver grid/surface-embedded silver nanowire hybrid structure," ACS Appl. Mater. Interfaces **8**(40), 27035–27043 (2016).
19. M. Mohl, A. Dombovari, R. Vajtai, P. M. Ajayan, and K. Kordas, "Self-assembled large scale metal alloy grid patterns as flexible transparent conductive layers," Sci. Rep. **5**(1), 13710 (2015).

Optics EXPRESS

20. S. Hong, H. Lee, J. Lee, J. Kwon, S. Han, Y. D. Suh, H. Cho, J. Shin, J. Yeo, and S. H. Ko, "Highly stretchable and transparent metal nanowire heater for wearable electronics applications," Adv. Mater. **27**(32), 4744–4751 (2015).
21. A. Khan, S. Lee, T. Jang, Z. Xiong, C. Zhang, J. Tang, L. J. Guo, and W. D. Li, "High-performance flexible transparent electrode with an embedded metal mesh fabricated by cost-effective solution process," Small **12**(22), 3021–3030 (2016).
22. Q. Peng, S. Li, B. Han, Q. Rong, X. Lu, Q. Wang, M. Zeng, G. Zhou, J.-M. Liu, K. Kempa, and J. Gao, "Colossal figure of merit in transparent-conducting metallic ribbon networks," Adv. Mater. Technol. **1**(6), 1600095 (2016).
23. B. Han, K. Pei, Y. Huang, X. Zhang, Q. Rong, Q. Lin, Y. Guo, T. Sun, C. Guo, D. Carnahan, M. Giersig, Y. Wang, J. Gao, Z. Ren, and K. Kempa, "Uniform self-forming metallic network as a high-performance transparent conductive electrode," Adv. Mater. **26**(6), 873–877 (2014).
24. S. Kiruthika, K. D. M. Rao, A. Kumar, R. Gupta, and G. U. Kulkarni, "Metal wire network based transparent conducting electrodes fabricated using interconnected crackled layer as template," Mater. Res. Express **1**(2), 026301 (2014).
25. Y. Han, J. Lin, Y. Liu, H. Fu, Y. Ma, P. Jin, and J. Tan, "Crackle template based metallic mesh with highly homogeneous light transmission for high-performance transparent EMI shielding," Sci. Rep. **6**(1), 25601 (2016).
26. B. Seong, H. Yoo, N. Vu Dat, Y. Jang, C. Ryu, and D. Byun, "Metal-mesh based transparent electrode on a 3-D curved surface by electrohydrodynamic jet printing," J. Micromech. Microeng. **24**(9), 097002 (2014).
27. T. Gao, B. Wang, B. Ding, J. K. Lee, and P. W. Leu, "Uniform and ordered copper nanomeshes by microsphere lithography for transparent electrodes," Nano Lett. **14**(4), 2105–2110 (2014).
28. Y. Liu, S. Shen, J. Hu, and L. Chen, "Embedded Ag mesh electrodes for polymer dispersed liquid crystal devices on flexible substrate," Opt. Express **24**(22), 25774–25784 (2016).
29. M. M. Menamparambath, C. M. Ajmal, K. H. Kim, D. Yang, J. Roh, H. C. Park, C. Kwak, J.-Y. Choi, and S. Baik, "Silver nanowires decorated with silver nanoparticles for low-haze flexible transparent conductive films," Sci. Rep. **5**(1), 16371 (2015).
30. J. van de Groep, P. Spinelli, and A. Polman, "Transparent Conducting Silver Nanowire Networks," Nano Lett. **12**(6), 3138–3144 (2012).
31. R. Gupta, K. D. M. Rao, S. Kiruthika, and G. U. Kulkarni, "Visibly Transparent Heaters," ACS Appl. Mater. Interfaces **8**(20), 12559–12575 (2016).
32. P. Li, J. Ma, H. Xu, X. Xue, and Y. Liu, "Highly stable copper wire/alumina/polyimide composite films for stretchable and transparent heaters," J. Mater. Chem. C Mater. Opt. Electron. Devices **4**(16), 3581–3591 (2016).
33. A. Y. Kim, M. K. Kim, C. Hudaya, J. H. Park, D. Byun, J. C. Lim, and J. K. Lee, "Oxidation-resistant hybrid metal oxides/metal nanodots/silver nanowires for high performance flexible transparent heaters," Nanoscale **8**(6), 3307–3313 (2016).
34. Y. Kim, H. R. Lee, T. Saito, and Y. Nishi, "Ultra-thin and high-response transparent and flexible heater based on carbon nanotube film," Appl. Phys. Lett. **110**(15), 153301 (2017).